Title	Tailoring cocrystal and salt formation and controlling the crystal habit of diflunisal
Author(s)	Pallipurath, Anuradha R.; Civati, Francesco; Eziashi, Magdalene; Omar, Elaf; McArdle, Patrick; Erxleben, Andrea
Publication Date	2016-09-26
Publication Information	Pallipurath, Anuradha R., Civati, Francesco, Eziashi, Magdalene, Omar, Elaf, McArdle, Patrick, & Erxleben, Andrea. (2016). Tailoring Cocrystal and Salt Formation and Controlling the Crystal Habit of Diflunisal. Crystal Growth & Design, 16(11), 6468-6478. doi: 10.1021/acs.cgd.6b01154
Publisher	American Chemical Society
Link to publisher's version	http://dx.doi.org/10.1021/acs.cgd.6b01154
Item record	http://hdl.handle.net/10379/6535
DOI	http://dx.doi.org/10.1021/acs.cgd.6b01154

Tailoring Co-crystal and Salt Formation and Controlling the Crystal Habit of Diflunisal

Anuradha R. Pallipurath, Francesco Civati, Magdalene Eziashi, Elaf Omar, Patrick McArdle,* and Andrea Erxleben*

School of Chemistry, National University of Ireland, Galway, Ireland

*Corresponding author email address: andrea.erxleben@nuigalway.ie (AE);

p.mcardle@nuigalway.ie (PM)

Abstract

Crystal habit modification of the drug diflunisal that normally grows into extremely thin, long needles has been achieved by breaking the stacking effect with the help of co-formers. Eight new co-crystals are reported, along with three crystal structures. In all cases, ortho F disorder, often a feature in diflunisal structures was absent due to the presence of CH…F interactions. Co-milling diflunisal with oxalic acid produced 1:1 and 2:1 co-crystals. In contrast, in solution crystallisation oxalic acid played the role of an additive resulting in the crystallisation of diflunisal form I rather than form III. To rationalize co-crystal formation a statistical analysis of the CCDC data base for aromatic o-hydroxy carboxylic acids was carried out. All co-crystals of o-hydroxy carboxylic acids with the COOH dimer motif have an electron-withdrawing group on one of the acids. COOH…N_{ar} motifs are formed preferentially over carboxylic homo-dimers in the presence of an N_{ar} co-former.

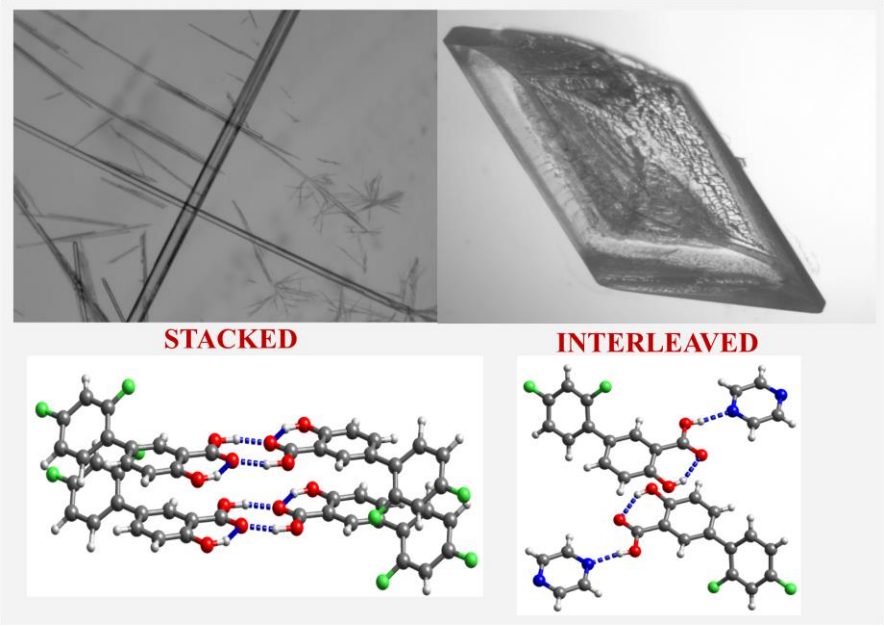

Tailoring Co-crystal and Salt Formation and Controlling the Crystal Habit of Diflunisal

Anuradha R. Pallipurath, Francesco Civati, Magdalene Eziashi, Elaf Omar, Patrick McArdle,* and Andrea Erxleben*

School of Chemistry, National University of Ireland, Galway, Ireland

*Corresponding author email address: andrea.erxleben@nuigalway.ie (AE);

p.mcardle@nuigalway.ie (PM)

Abstract

Crystal habit modification of the drug diflunisal that normally grows into extremely thin, long needles has been achieved by breaking the stacking effect with the help of co-formers. Eight new co-crystals are reported, along with three crystal structures. In all cases, ortho F disorder, often a feature in diflunisal structures was absent due to the presence of CH…F interactions. Co-milling diflunisal with oxalic acid produced 1:1 and 2:1 co-crystals. In contrast, in solution crystallisation oxalic acid played the role of an additive resulting in the crystallisation of diflunisal form I rather than form III. To rationalize co-crystal formation a statistical analysis of the CCDC data base for aromatic o-hydroxy carboxylic acids was carried out. All co-crystals of o-hydroxy carboxylic acids with the COOH dimer motif have an electron-withdrawing group on one of the acids. COOH…N_{ar} motifs are formed preferentially over carboxylic homo-dimers in the presence of an N_{ar} co-former.

Keywords: Diflunisal, co-crystals, Gaussian, stacking analysis, crystal morphology, PIXEL

Introduction

Needle like crystals of drugs not only tend to have dissolution issues, but are also known to pose a challenge to processing because they have poor flow properties and form tablets of variable densities.[1] Diflunisal (**Chart 1**) which is used for the treatment of rheumatoid arthritis[2] and chronic lower back pain[3] readily crystallizes as acicular needles which are difficult to handle.

Improving the physicochemical properties of drugs can often be achieved through the use of techniques like co-crystallisation,[4,5] milling,[6] using supercritical fluids,[7] use of additives[8] and changing pH.[9] Co-crystallisation techniques have been widely employed to improve many properties of materials like colour,[10] fluorescence[11,12] and the bioavailability of drugs.[13] While various techniques like liquid assisted grinding,[14] use of phase diagrams,[15,16] and thermochemistry[17,18] are used for experimental co-crystal screening, predicting co-crystallisation success is still quite a challenge.

Extensive efforts are being made to understand the selection rules behind the formation of co-crystals, but there are still no universal criteria for algorithms that help predict the likelihood of co-crystal formation.[18] Grecu *et al*. have used interaction site pairing energies as a method of virtual screening for the co-crystallisation of nalidixic acid[19] and various other systems.[20] Springuel *et al.* carried out conformational analysis and virtual co-crystal screening through identifying the structural resemblance of potential co-formers with those already known to form co-crystals with drug molecules.[21] Multipolar refinements were carried out to try to understand the influence of inter- and intra-molecular H-bonding on the interaction energies that define the co-crystal – salt continuum.[22] *Ab initio* DFT-D methods have been used to successfully predict 99 out of 102 structures, studied by Chan *et al*. using calculated thermodynamic stabilities relative to those of the starting materials.[23]

Tools like Molecular Complementarity[24] in the Mercury software[25] take advantage of the vast collection of crystal structures in the CSD database to give a statistical prediction of possible co-crystallisation events. Hydrogen bond propensity calculations have been used to quantify H-bonding in intra- and inter-molecular situations.[26] While this approach is successful in many cases, it cannot predict situations where there is no direct interaction between the components, and also situations where adduct formations are a result of mere solubility differences.[27]

Even though these tools have come a long way in predicting the role of a molecule as a co-crystalliser, there is still little understanding of the energetics and the kinetics involved in the formation of these systems. Empirical rules for co-crystallisations[14,28] suggest that a pK_a difference that is close to 0 between the two molecules under study would give rise to a co-crystal, while a ΔpK_a value between 0 and 3.75 would give rise to inter-molecular H-bonding that has no clear ionic or covalent nature. On the other hand, a ΔpK_a value greater than 3.75 should lead to proton transfer and salt formation. Lemmerer *et al.* have predicted co-crystal or salt formation between carboxylic acids and pyridine by calculating their pK_a and other differences.[29] This study did not extend to the case of ortho-hydroxy

substituted benzoic acids. Many of the non-steroidal anti-inflammatory drugs (NSAID), like diflunisal, aspirin, salisalate, piroxicam and other salicylic acid derivatives are of this type and it has been pointed out that the introduction of the ortho-hydroxy group can have a profound influence due to its resonance, steric and H-bonding effects.[30] Fiedler *et al.* through titrimetry and density functional studies, established that intra-molecular H-bonding has a great influence on the acidity of ortho-substituted benzoic acids,[31] while they however, could not separate the influence of hydrogen-bonding and steric effects on this so called 'ortho effect'. Competition between intra- and inter-molecular H-bonding can greatly influence the ability of a synthon to form a co-crystal. Understanding these systems will help develop empirical rules for their co-crystallisation to improve their physical properties.

Nine co-crystals of diflunisal are known but only three crystal structures have been reported. In all cases diflunisal forms 2:1 adducts with the co-formers, with up to twice the bioavailability.[13] Wang *et al.* established the presence of COOH…NCO adduct formation through FTIR and solid state NMR studies of diflunisal-nicotinamide and isonicotinamide co-crystalline adducts in the absence of a crystal structure.[32] A diflunisal-nicotinamide co-crystal was obtained using supercritical CO_2.[7] The crystal structures of co-crystals containing two active pharmaceutical ingredients (APIs), diflunisal and ciprofloxacin,[33] and of diflunisal-theopylline[34] have also been reported. Evora *et al.* carried out co-crystal screening of diflunisal with isomeric pyridine carboxamides using phase diagrams, which resulted in three new crystalline adducts, whose interactions were estimated using peak shifts in the FTIR spectrum.[16] Evora *et al.* also made use of thermomicroscopy to study a new phase of a diflunisal-pyrazinamide co-crystalline adduct.[17]

Another technique for improving the dissolution properties and processability of an API is a change in crystal morphology. Sometimes, this can be achieved through co-crystallisation. The use of additives or the presence of impurities are also known to lead to changes in the crystal habit. An additive that interacts only with a specific crystal surface can give a kinetically controlled metastable polymorph, while thermodynamic stabilisation in the presence of an additive can be achieved by the solvent co-adsorption phenomena.[35] An additive that is structurally similar to the compound being crystallised may disrupt both nucleation and crystal growth.[36]

In this paper we identify key interactions involved in the formation of diflunisal adducts with co-formers through statistical, theoretical and experimental methods. We have used a molecular similarity tool to predict possible co-formers and carried out co-crystallisation experiments to obtain crystalline adducts that are not subject to the crystal growth process accelerated by vdW contact stacking which often leads to the formation of needles. We also studied the inter-molecular interactions using DFT-D calculations for adducts in the gas phase and used PIXEL calculations to partition inter-molecular interaction energies in the co-crystals. We have also accessed a range of co-

crystal adducts of diflunisal with carboxylic acids through mechanochemistry, which were considered unlikely by the molecular complementarity tool.

Experimental Section

Materials

Diflunisal (**1**) was purchased from Baoji Guokang Bio-Technology Co., Ltd, China. The solvents, pyrazine (Py - **a**), 1,3-di (4-pyridyl) propane (PBipy - **b**), 4-(2-pyridine-4-ethyl) pyridine (EBipy – **c**), 4,4'-bipyridine (Bipy – **d**), oxalic acid (OA – **e**), 4-aminobenzoic acid (PABA – **f**), 2-hydroxypyridine (HP – **g**), citric acid (CA - **i**), DL-tartaric acid (TA - **j**), DL-malic acid (DLMA - **k**), L-ascorbic acid (AA - **l**), *trans*-aconitic acid (tAA - **m**), adipic acid (APA - **n**), succinic acid (SA - **o**), maleic acid (MA - **p**), glutaric acid (GA - **q**), pimelic acid (PA - **r**), and fumaric acid (FA - **s**) were purchased from Sigma Aldrich. 4-Diamino-6-hydroxypyrimidine (DAHP - **h**) was purchased from Tokyo Chemical Industry (TCI, Europe). All chemicals were used without any further purification.

Solution co-crystallisation

1:1 molar ratios of **1** and the co-formers **a** (Py), **b** (Pbipy) and **c** (Ebipy) were dissolved in methanol/acetonitrile (1:1), with stirring and gentle heating. Crystalline adducts were obtained through slow evaporation of the solvent mixture. Similar experiments were carried out using other co-formers but were unsuccessful in producing single crystals. To study the additive effect of **e** (OA), **1** and 10 % **e** were dissolved in ethanol, both with stirring and gentle heating, followed by slow evaporation.

Ball milling

Ball milling experiments with a 1:1 ratio of **1** and co-formers **e**-**s** and 1:1 and 2:1 ratios for the dipyridyl co-formers (**b**-**d**) and Py (**a**) were carried out at various time intervals, at 25 Hz using a Retsch ball mill. For long duration of milling the jars were allowed to cool for 15 min after every 30 min milling. Cryo-milling was carried out on 1:1 combinations of **1** and the carboxylic acid co-formers using the same mill, for different times. The jars were initially immersed in liquid nitrogen for 5 min and the millings were carried out in intervals of 7.5 min and the jars were cooled in between for 2.5 min. The measured external temperature of the jars did not rise above -20 °C during cryo milling.

Single crystal X-ray diffraction

Single crystal diffraction data of all crystalline adducts were collected using an Oxford Diffraction Xcalibur CCD diffractometer using graphite-monochromated Mo-Kα radiation (λ = 0.71073 Å) at

room temperature (**1a**) or 150 K (**1b**, **1c**). The structures were solved using SHELXT,[37] embedded in the OSCAIL software.[38] Non-hydrogen atoms were refined anisotropically and hydrogen atoms were in calculated positions. Graphics were produced with ORTEX and POGL also embedded in OSCAIL. Crystallographic data can be found in **Table 1**. CIF files can be obtained free of charge at www.ccdc.cam.ac.uk/conts/retrieving.html or from the Cambridge Crystallographic Data Centre, Cambridge, UK with the REF codes 1491984, 1491985, and 1491986.

X-ray powder diffraction (XRPD)

X-ray powder patterns were recorded on an Inel Equinox 3000 powder diffractometer between 5 and 90 ° (2θ) using Cu K_α radiation (λ = 1.54178 Å, 35 kV, 25 mA). Theoretical powder patterns were calculated using the OSCAIL software.[38]

Differential scanning calorimetry (DSC)

DSC experiments were performed on a STA625 thermal analyzer from Rheometric Scientific (Piscataway, New Jersey). The heating rate was kept constant at 10 °C/min and all runs were carried out between 25 °C and 250 °C. The measurements were made in open aluminium crucibles, nitrogen was purged in ambient mode and calibration was performed using an indium standard.

Scanning electron microscopy (SEM)

The images were captured using a Hitachi S2600N Variable Pressure Scanning Electron Microscope with a backscatter BSE resolution of 20 nm at 25 kV, X 903 magnification, with an accelerating voltage of 5 kV, an emission current of 10000 nA at a working distance of 13.5 mm.

Computational studies

Molecular complementarity

The Molecular Complementarity tool in the Mercury software[25] was used to identify potential co-formers for the co-crystallisation of **1**. This was carried out using the database of potential targets supplied by the database, and a few other structures were loaded as their .mol files saved using the Avogadro software.[39]

CSD search for motifs

A motif search for three types of H-bonded adducts shown in **Chart 2** was carried out, using the Conquest software.[40] One moiety in each case was an ortho-hydroxy benzoic acid, while the second moiety was either a structure with an aromatic N, forming a 1D hydrogen bond with the acid or another carboxylic acid group forming a dimer with the acid. The criteria used for the search were that the interactions are within a distance of the sum of the vdW radii +1 Å, an R-factor < 7.5%, and organometallics were excluded. The results, in the form of descriptors, from the searches were then

exported to the Mercury software, where descriptive statistical analysis and principal component analysis[41] of Z', hydrogen bonding distances, number of unique chemical units, and the number of co-ordinates were carried out.

Gaussian calculations

Gaussian calculations were carried out on the individual molecules (**1**, **a** – **e**) and their adducts with a subset of the co-formers (**a – e**), in the gas phase, using density functional theory (DFT). The B3LYP functional was employed with two different basis sets, 6-311+g(d,p) and cc-pvtz. The structures were optimised for lowest energy and checked for the absence of negative frequencies. Simple formation energies were calculated from the minimized energies.

Stacking analysis

Stacking analysis[1] was performed on the obtained structures using OSCAIL.[38] The vdW distances of a molecule to its nearest neighbours in potential stacks were calculated.

PIXEL calculations

PIXEL calculations[42] were carried out to examine the contributions of various interactions towards the stability of the crystalline adduct **1a**, of the crystal structure of **1** (REF code: **FAFWIS01**) and of co-formers **a** (REF code: **PYRAZI**), **b** (REF code: **AZSTBB**), **c** (REF code: **UGIHAT**), **d** (REF code: **HIQWEJ**), and **e** (α form REF code: **OXALAC05**, β form REF code: **OXALAC11**). In the case of **1**, one disordered F in the structure was replaced with a H to simplify the calculation. PIXEL calculations on the other crystalline adducts were not possible as they had a Z' > 2.

Results and Discussion

The promiscuity of drug molecules in co-crystal formation and the efficient use of supramolecular synthons have been a topic of wide interest for the past decade. Shattock *et al.*[43] in their study of the heterosynthon motif OH…N_{ar} carried out an examination of the crystal structures in the CSD and established that a COOH…N_{ar} 1D H-bond is preferred over OH….N_{ar}. However, they did not include species with ortho substitution due to their complexity. Amongst the 4922 structures in the CSD that have the COOH…COOH homosynthon, 149 of them have a hydroxyl group in the ortho position (motif **II**), equivalent to only 3% of the total. Similarly, a search for COOH…N_{ar} gave 1780 hits out of which 82 had a hydroxyl group in the ortho position (motif **I**). Adduct formation is known to prefer heterosynthons over homosynthons in the process of H-bond formation,[28] but only a COOH homodimer can be broken using a heterosynthon, while an amide homodimer in contrast is considered quite stable. Hence, here we have compared only ortho substituted COOH homosynthons to N_{ar} heterosynthons.

Out of the 149 structures, identified as having motif **II**, only eight were co-crystals. From an examination of these structures, the following features were identified:

1) COOH homosynthons between a co-former acid and an o-hydroxy carboxylic acid formed when either of them had electron-withdrawing groups present. Examples are **REFCODES BIZYOA** and **COLKUL**, which have chloroacetic acid and dinitrobenzoic acid as co-formers. The presence of electron-withdrawing groups would greatly enhance the proton donating ability of the carboxylic acids. The pK_a values are listed in **Table S1** (Supporting Information, SI). The only co-former that does not have an electron-withdrawing group is acetic acid (**REFCODES: YOVVOW, MAMRUP, MAMSAW**).
2) COOH homosynthons between a co-former acid and an o-hydroxy carboxylic acid formed when the o-hydroxy acid had a competing group (OH or NH_2) that can H-bond with the co-former. Examples are **REFCODES GEQROL, GIDLUB, UGOWIY**.

A search that combined motifs **I** and **II** gave only eight hits, and in every single case the COOH…COOH distances were greater than 3 Å excluding a planar $R_2^2(8)$ motif. The normal distance for COOH…COOH interactions is around 2.6 Å.[43]

Out of the 149 structures with the type **II** interactions, 49 showed stacking with the stacks slightly slipped. In the case of the COOH…N_{ar} interactions (motif **I**), out of the 82 that have the o-hydroxy acid, 23 are stacked. Survo *et al.* found rare type **III** interactions in the co-crystals of **1** with theophylline. A search on the CSD for structures with motif **III** gave 78 structures, of which only 20 were actually in-plane interactions.

We carried out principal component analysis (PCA) on our searches based on motifs **I** and **II** in **Chart 2** separately, using the tools available in Mercury. The descriptors used for the PCA were Z', distances (the H-bond distances between the H and the acceptor – 1 length in motif **I** and 2 in motif **II**), the number of atomic co-ordinates in the unit cell, and the number of unique chemical units.

The COOH… N_{ar} interactions: The PCA gave a cumulative variance of 100% for the first four PCs. PC1 (49.4% explained variance) was influenced surprisingly by Z' and the number of co-ordinates, PC2 (24.7% explained variance) has a contribution from the number of unique chemical units. This is apparent from **Figure 1a**, where the data points are sorted into three distinct layers along the y-axis denoting PC2. It is only PC3 (18.5% explained variance), perhaps surprisingly, that has any contribution from the H-bonding distances. This is because the COOH…N distances are very consistent (1.6 – 1.8 Å) and thus do not contribute to variance. There are three exceptions here that have distances in the range of 2.3 - 2.6 Å. However, these systems contain pyridine N-oxide.[44]

The COOH…COOH interactions: PCA gave a cumulative explained variance of 99% for the first four PCs. PC1 (46.8% explained variance) has the highest contribution from the hydrogen bonding

distances, as can be seen from **Figure 1b**, with all the data points with a star marker clustering to one side. PC2 (32.98% explained variance) is related to the difference in the two H-bonding distances that make the dimer ring, and PC3 (14.64% explained variance) is governed by the number of unique chemical entities in each studied molecule. PC4 (5.4% explained variance) is related to Z' and the number of co-ordinates had no significance whatsoever.

Gavezzotti *et al.* in a recent study have carried out a survey of all H-bonded structures and have explored the H-bonding features and the nature of crystal packing amongst other features. They found the order of donor ability to be COOH > NH > OH, with the COOH…N_{ar} being the most favourable of interactions.[45]

Studies based on diflunisal

Molecular complementarity calculations revealed that **1** was likely to form co-crystals with co-formers which had 'N' acceptors, rather than dicarboxylic acids, with exceptions of adipic acid (**n**) and benzoic acid (not studied here). This method makes use of multivariate analysis of the structures in the database, and projecting the current data to find a possible co-crystallisation hit. The data used are various properties, as well as crystallographic information.[24] **Table S2** (SI) lists the possible hits predicted using this method. These predictions were tested by carrying out a series of co-crystallisation studies by ball milling and solution crystallisation of **1** with the co-formers listed above.

Solution crystallisation

Crystals of **1a** (Dif-Py), **1b** (Dif-Pbipy), and **1c** (Dif-Ebipy) were obtained from a mixture of 1:1 acetonitrile and methanol and the crystal habits were distinctly different from that of **1**, especially in the case of **1a** and **1b**. The crystallographic information for **1a-1c** are summarised in **Table 1**. **Figure 2** illustrates the crystal packing observed in **1a**, **1b** and **1c**. While **1a** is a co-crystal, **1b** and **1c** are salts where the proton from the carboxylic acid has been transferred to the N in the co-former. In all three cases the H bonding motifs observed are linear chains of the co-formers with a molecule of **1** at both ends. This is due to competition between inter- and intra-molecular H-bonding possibilities present in the molecule of **1**.

As can be seen from **Figure 3a**, **1a** has a diamond-like habit. The crystal structure has an interleaved pattern with two molecules of **1** spaced by an **a**, with a **1-a** distance of 3.7 Å. **Figure 3b** shows that **1b** forms plate like crystals, crystallising in a monoclinic ($P2_1/c$) system. It has a rather large unit cell, which comprises of one molecule of **b** and two molecules of **1**, with the ring carrying the carboxylic acid in **1** being co-planar to the pyridyl rings in **b**. **1c** on the other hand forms needles like **1** itself does, and crystallises in the triclinic (P-1) system. **1c** also has a molecule of the solvent acetonitrile

included in its unit cell. **1a** and **1c** are stable, while **1b** is very hygroscopic and is unstable when the solvent is removed.

To understand the direction and mechanism of growth in these systems, stacking analyses were carried out using the OSCAIL software.[1] **Table 2** gives a comparative account of the percentage of vdW interactions observed in the crystal lattices along all axes. For a stacking interaction to dominate crystal growth it is normally found that more than 50% of the atoms in a molecule are in vdW contact with their neighbours above and below them in a stack.[1] In the case of the crystal form of **1**,[46] the crystal growth is dominated by the vdW contact stacking of the molecules along the short *a*-axis, resulting in needle formation. **1c** is similar; here the growth is dominated by the vdW contact stacking of **c** on **c** and **1** on **1**, and 84% of the atoms in the molecules are in vdW contact with their neighbours in the stack along the *b* axis. The acetonitrile solvent molecules in **1c** fill voids and play no role in stacking. In the case of **1a**, vdW interactions involving molecules along the a and c axes have only 43.5% and 35.6% of their atoms in vdW contact, respectively. There is obvious interleaving of non-identical molecules along b and c and the vdW contact stacking mechanism cannot contribute to growth in these directions. In the case of **1b** the molecules have only 21% of their atoms in vdW contact along the relatively short b-axis and needle growth is not expected. A possible reason for the **1c** structure being related to that of **1** is that **1** and **c** are closely related in size and shape.

Another interesting feature of these crystalline adducts is the absence of disorder with respect to the F atoms of **1**. In the crystal structures of **1** (form I - **FAFWIS01** and form IV – **FAFWIS**) the ortho F atom is disordered. This apparent disorder is due to the availability of space for torsion of the F-carrying phenyl ring. In **1a**, **1b** and **1c**, the ortho F is present on the side having the carboxylic acid unit in the adjacent ring. The formation is such that there is a pocket of C-F and C-H bonds, with the shortest C-H…F distance being 2.5 Å and largest F – F distance 5 Å and shortest 3.68 Å. Usually an F…H interaction is not considered significant due to the nature of F,[47] but here the short C-H…F distance, 2.5 Å, indicates a weak interaction (vdW sum 2.67 Å) that seems to be vital in preventing the disorder. In rare occasions, aromatic fluorine substitutions, due to the weak F…H interactions can affect optimal geometries of structures.[47] Such a feature was also identified by Bag *et al.*[33] in co-crystals of **1** with ciprofloxacin, where the weak C-F…H interactions form tetrameric units. Illustrative figures with measured distances are in the SI (**Figure S3**). The **FAFWIS01** structure which has ortho F disorder has been compared to the **FAFWIS02 (**diflunisal form III**)**, **1a, 1b** and **1c** structures which have no F disorder by placing an F atom along the C-H vector where an F atom would be if there was disorder. The lattice around the inserted F atom was examined for contacts inside the sum of the vdW radii. The results were that in **FAFWIS01** neither F position made any contacts inside the sum of the vdW radii while the inserted F atom in all of the other four structures made contacts inside the sum of the vdW radii (**Table S3**).

PIXEL calculations were carried out on **1a**, **1**, **a**, **b**, **c**, **d**, and two forms of **e** to identify important interactions and their respective contributions to the stability of the structure. It was not possible to carry out the calculations on structures of **1b** and **1c**, because their Z' >2 is beyond the computational limitations of the code.[42] **Table 3** lists the interaction energies of a central molecule of **1** with its next nearest neighbours in the co-crystal **1a**. PIXEL energies for **1** and the co-formers (**a – e**) can be found in the SI **(Tables S4 – S10)**. On comparison of the energy involved in **1** (-114.5 kJ/mol) with that of **a** (-59.7 kJ/mol) and **1a** (-63.9 kJ/mol), it becomes apparent that there is no thermodynamic advantage for the formation of the co-crystal, as reported in the literature by Chan *et al.* using DFT-D methods.[23] Gavezzotti *et al*. in their recent study[45] surveyed the CSD for co-crystals and carried out CLP calculations on 97 structures. They found that the lattice energies of the co-crystals were invariably more stabilising than the lattice energies of the components themselves. Their finding would suggest that even though the formation energies of the hetero-adducts are higher than that of their individual components, there is increased stability due to crystal packing effects. Unfortunately, they were not able to survey pharmaceutical co-crystals in any great length due to the presence of multiple functional groups.

While dispersion energies are dominant in the crystal structure of **a**, combined with the fact that it has low lattice energies, gives it an advantage in forming **1a.** The crystal structure of **1** is however, dominated by the Coulombic energy of the $R_2^2(8)$ H-bond dimer it forms with itself, followed by the dispersion energy of stack formation. **Figure 4** illustrates the interactions observed in the **1a** crystal, showing the origin of the dispersion and Coulombic energies.

DFT calculations on the H-bonded adducts studied using Gaussian reveal a similar result. The formation energies calculated for adducts are much smaller than that of the **1-dimer**, except for the case of the **1-e** adduct, which had very similar formation energies to that of the **1-dimer** itself. The formation energies for all adducts can be found in **Table S11** (SI). It has to be noted that the gas phase calculations do not take the proton transfer in **1b** and **1c** into account, *i.e.* the formation of charge-assisted H bonds. Arderne *et al*. through their calculations have shown that charge-assisted H-bonding tends to give adducts an extra 13 – 14 kJ/mol stabilisation compared to their neutral versions.[48] Adding in the extra 13 kJ/mol to the formation energies of **1b** and **1c** would still make their formation energy similar to and slightly higher than that of **1** itself. The fact that these adducts have lower formation energies suggests that their formation may well be driven by entropy, which would favour a heterosynthon over a homosynthon. It would also suggest that, being less stable than **1** itself, the adducts should have enhanced dissolution properties and hence be more bioavailable. In the case of oxalic acid the formation energies were very similar to that of the **1-dimer** and yet it did not produce co-crystals in solution. In this case, there is no advantage in terms of formation energies due to the presence of COOH…COOH dimers and the entropy difference should also be small.

While further crystallisation studies were carried out using the other co-formers, they were not successful in producing co-crystals or salts. However, oxalic acid (**e**) had an interesting effect in the crystallisation of **1**. **1** is known to produce crystals of polymorph III (FIII) in pure ethanol.[46] However, in the presence of 10-50 % oxalic acid we observed the formation of form I (FI) in the same solvent. FI was identified by indexing single crystals on a diffractometer. FI is generally crystallised from toluene or from a mixture of benzene and methanol.[46] Using **e** as an additive this polymorph can be obtained from the greener solvent ethanol. Thomas *et al*. have made similar observations in the cases of paracetamol,[49] piroxicam,[50] and gallic acid,[50] where the presence of a large amount of co-former led to the formation of rare or previously unknown polymorphs. However, they have not been able to identify a mechanism for this behaviour. Due to large quantities of the co-former required, as opposed to the small amounts of additives generally known to affect nucleation events, we hyptothesize that the effect of the co-former might actually be a crystal growth effect.

Together with the experimental observations and the findings of the DFT calculations showing very similar formation energies for both the **1** homodimer and **1e** hetero-adduct, it would seem that, in the presence of a co-former, the increase in entropy presents no advantage for the formation of co-crystals, as the enthalpy of formation dominates the thermodynamics of the system. It has been observed through ball milling (which we discuss in the next section), that **1e** co-crystals are formed on milling. This would suggest that the co-crystal may have very high solubility at room temperature, preventing its crystallisation. The reason for large quantities of co-former causing a change in polymorph of the drug, is not currently understood, but further studies on this phenomenon are being carried out.

After a few months in contact with solution, a few plates of FIV were also found amongst the FI needles. In the absence of oxalic acid FIV rapidly crystallises as needles. The transformation to the more thermodynamically favoured plates is a slow process. Previously, alkanoic carboxylic acids have been used as additives by Davey et al.[51] in small quantities to modify the morphology of adipic acid. They observed an increase in the aspect ratio of the crystals, eventually leading to the formation of twin crystals of adipic acid in the presence of alkanoic acid. A long established example is that of urea modifying the morphology of NaCl crystals. Smith *et al*. have recently carried out theoretical and computational studies to understand the effect urea has on crystal growth.[52] They identify that urea preferentially stabilises octahedral NaCl, by raising the chemical potential of all faces; however, the 111 face was the most stable.

Ball milling

Mechanochemistry, due to its non-equilibrium nature, is often employed to produce polymorphs[6] and co-crystals[53] that are not accessible through solution crystallisation. Ball milling of **1** with all of the co-formers was carried out initially for 60 min. It was possible to produce eight new co-crystals by

this method. The results of the ball milling experiments are summarised in **Table 4**. Co-milling of a 2:1 mixture of **1** and **a** (Py) for 15 min resulted in an XRPD pattern similar to the simulated pattern from the single crystal data (**Figure S2**), suggesting the formation of the same co-crystal. Co-milling 1:1 and 2:1 ratios of **1** and **b** (Pbipy) for 30 min resulted in a physical mixture, while milling in the presence of 25 μL of acetonitrile produced the same XRPD pattern as that simulated from the single crystal data (**Figure S4**). The added acetonitrile is required, as proton transfer cannot take place in the absence of a solvent. This effect has been previously reported.[53] Thermal analysis (**Figure S5**) of the milled material showed melting at 151 °C with no other thermal events except for sublimation at a higher temperature.

Co-milling 1:1 and 2:1 mixtures of **1** and **c** (Ebipy), gives rise to new XRPD patterns (>5 new peaks per pattern, **Figure S6**) that are different to the ones simulated from the single crystal structures. This observation is supported by thermal analysis (**Figures S7** and **S8**, SI), which shows a thermal event in both cases at 145 – 146 °C and melting endotherms at 239 °C and 229 °C for the 1:1 and 2:1 samples, respectively. The melting points of the different polymorphs of **1** are between 212 and 215 °C [46] and that of **c** is at 151 °C. There is a thermal event at 86 °C in the 2:1 case, the origin of which is not currently understood. The absence of the melting endotherms of the starting compounds and the differences in the XRPD patterns support the presence of pure co-crystals. Samples of **1a**, **1b** and **1c** prepared by milling are stable for over two months.

The XRPD patterns of milled 1:1 and 2:1 mixtures of **1** and **d** (Bipy), both having >5 new peaks (**Figure S9**, SI), suggest the formation of new co-crystalline adducts. Thermal analysis of the milled 2:1 mixture shows an exothermic peak at 127 °C, followed by melting at 202 °C (**Figure S10**, SI). The absence of a melting endotherm for **d** (m.p. 114 °C) complements the XRPD data.

XRPD patterns of 1:1 mixtures of **1** and **f** (PABA), milled at room temperature or cryo-milled for 120 mins, are completely different compared to the starting materials and have a few peaks that distinguish them from each other (**Figure S11**). The pattern of the cryo-milled sample shows Bragg peaks with an underlying amorphous halo contributed from diffuse scattering. Thermal analysis of a sample milled at room temperature confirmed the formation of a new co-crystalline material, with a thermal event at 115 °C followed by melting at 165 °C. The melting point of **f** is 187 °C (**Figure S12**, SI).

Co-milled **1** and **g** (HP) in a 1:1 ratio results in a new XRPD pattern (**Figure S13**, SI) suggesting the formation of a new co-crystalline adduct. This is further supported by the thermal analysis (**Figure S14**, SI) where the material shows an endothermic peak at 187 °C, followed by melting at 202 °C. These thermal events are different from the starting materials, where **g** is known to melt at 107 °C. HP exhibits lactam-lactim tautomerism. Both tautomers can interact with a carboxylic acid *via* an $R_2^2(8)$ motif.

The case of oxalic acid (**e**) is very interesting. While the molecular complementarity tool in the Mercury software predicted a 0% probability of co-crystal formation, ball milling of 1:1 ratios of **1** and **e** resulted in a new pattern as shown in **Figure 5**, suggesting the formation of a 1:1 adduct. Thermal analysis of the milled material revealed four thermal events, each with an associated weight loss (**Figure 6**). The peak at 67 °C corresponds to the loss of 1.5% adventitious water. The second event occurs at 171 °C, with a 15.5% weight loss, that corresponds to the loss of half of **e** present in the system. The third thermal event occurs at 199 °C, with a weight loss of 27.2%, that corresponds to the loss of all **e** molecules, followed by the melting of **1** at 213 °C. The absence of the melting endotherm of **e** (m.p. 202 – 203 °C) and the loss of half of **e** at 171 °C suggests the transformation of **1e** from a 1:1 composition to a 2:1 adduct. This is supported by the XRPD patterns. To understand the change in composition better, the 1:1 co-milled sample was held at 100 °C for 30 min and a second sample at 100 °C for 30 min followed by 30 min at 180 °C. The XRPD patterns (**Figure 5**) reveal the formation of both 1:1 and 2:1 adducts. Another experiment was carried out where a 1:1 mixture of **1** and **e** (dihydrate form) was milled for 120 min without any cooling interval. This resulted in a bright purple sample (**Figure S15**), which could suggest the presence of a high degree of disorder in the structure.[54] The XRPD pattern (**Figure 5**, **D**) is almost identical to that of FIII with the exception of a new peak at 21° (2θ). The thermal analysis however, revealed the presence of a co-crystal that melts at 178 °C, with two other recrystallisation events. Together with the fact that the material melts at a temperature different to that of its starting material and that there is no weight loss involved in either of the thermal events, it can be safely concluded that this is a polymorph of **1e**. Seeded crystallisation experiments using crystals from the milled sample were unsuccessful.

In contrast to all other co-milling experiments, milling a 1:1 mixture of **1** and **h** (DAHP) did not yield an XRPD pattern. Only an amorphous halo was observed and no Bragg peaks appeared during storage for over 6 months (**Figure S16**). It is possible that crystallisation was effectively blocked by the multi-functional **h**, which has three H-bond donors and two acceptors, which could stabilize an amorphous phase by disrupting the formation of the acid dimers.[55]

Figure 7 shows the SEM images of ball milled **1d** (2:1, 15 min), **1f** (1:1, 60 min), **1f** (2:1, 60 min) and **1h** (1:1, 30 min). Corresponding low magnification images are shown in **Figures S17 – S22** (SI). For **1d** and **1h** tape like structures grew from flat surfaces which formed due to the impact of milling. In both of the **1f** cases the samples are completely made up of these tape like features, with the 1:1 tapes slightly wider than the 2:1 ones. Some of these tapes are similar to the ones observed on milling **1** alone for 120 min (**Figure S17**, SI).

In the interesting case of **1e**, milling for 120 min without intermittent cooling (**Figure 8a**) seems to lead to some kind of melting resulting in an amorphous looking material, from which some tape like features are growing. The 1:1 sample milled for 60 min with intermittent cooling, followed by heating

at 100 °C (**Figure 8b**) shows features similar to those in **Figure 7**. The sample heated at 180 °C that results in the 2:1 adduct as established by DSC shows the formation of large well defined blocks or plank like crystals. This could be an effect of the annealing process which could have led to the formation of these blocks that deviate from the normal needle like structures.

Co-milling of **1** with carboxylic acids **i – s** did not yield any co-crystals. Co-milling **1** and **s** resulted in an X-ray amorphous material that crystallises back to its constituents. XRPD patterns for these samples are shown in **Figures S23 – S33** (SI). Cryo-milling of these systems gave results that were similar to the room temperature studies (data not shown). A discrepancy with the predictions of the molecular complementarity tool in the Mercury software is the non-occurrence of co-crystals of **n** and **r**, either through milling or solution crystallisation, despite a prediction with a 100% hit rate. This tool however, has been successful in predicting co-crystallisers for diflunisal in 11 out of 14 cases the exceptions being oxalic acid, adipic acid and pimelic acid.

Conclusions

Ball milling diflunisal with a range of bipyridines, *p*-aminobenzoic acid and oxalic acid led to the formation of eight co-crystals.

Solution crystallization of diflunisal with pyrazine gave a co-crystal (**1a**) and a salt with 1,3-di(4-pyridyl)propane (**1b**) both of which unlike diflunisal do not show needle growth. However, centrosymmetric 4-(2-pyridine-4-ethyl)pyridine gives a salt which does show needle growth. The different morphologies of **1a** and **1b** are due to the presence of the co-formers that have a size and shape different to that of diflunisal and that prevent the stacking of molecules that dominates growth in the case of diflunisal and its salt with 4-(2-pyridine-4-ethyl) pyridine.

Diflunisal FI that is normally crystallised from toluene can also be obtained from the greener solvent ethanol in the presence of 10% oxalic acid.

Gaussian calculations show that the formation energies of adducts of diflunisal with the pyridines examined are much lower than that of the diflunisal dimer itself suggesting that other factors such as crystal packing may be important in controlling co-crystal formation.

Acknowledgements

This work was supported by Science Foundation Ireland under Grant No. [12/RC/2275] as part of the Synthesis and Solid State Pharmaceutical Centre (SSPC). ARP would like to acknowledge ICHEC, Irish HPC system for computing time on the condominium access (nuig02) and Dr Jonathan Skelton

for helpful computing advice. The authors acknowledge the facilities and technical assistance of the NCBES Electron Microscopy unit within the Centre for Microscopy & Imaging at the National University of Ireland Galway, a facility that is funded by NUIG and the Irish Government's Programme for Research in Third Level Institutions, Cycles 4 and 5, National Development Plan 2007-2013.

Abbreviations

1, diflunisal; Py – **a**, pyrazine; PBipy – **b**, 1,3-di (4-pyridyl) propane; (EBipy – **c**), 4-(2-pyridine-4-ethyl) pyridine; Bipy – **d**, 4,4'-bipyridine; OA – **e**, oxalic acid; PABA – **f**, *p*-aminobenzoic acid; HP – **g**, 2-hydroxypyridine; DAHP – **h**, 4-diamino-6-hydroxypyrimidine; CA – **i**, citric acid; TA – **j**, DL-tartaric acid; DLMA – **k**, DL-malic acid; AA – **l**, L-ascorbic acid; tAA – **m**, *trans*-aconitic acid; APA – **n**, adipic acid; SA – **o**, succinic acid; MA – **p**, maleic acid; GA – **q**, glutaric acid; PA – **r**, pimelic acid; FA – **s**, fumaric acid.

References

(1) Walshe, N.; Crushell, M.; Karpinska, J.; Erxleben, A.; McArdle, P. *Cryst. Growth Des.* **2015**, *15*, 3235–3248.

(2) Brogden, R. N.; Heels, R. C.; Pakes, G. E.; Speight, T. M.; Avery, G. S. *Drugs* **1980**, *19*, 84–106.

(3) Berry, H.; Bloom, B.; Hamilton, E. B.; Swinson, D. R. *Ann. Rheum. Dis.* **1982**, *41*, 129–132.

(4) Lu, J.; Li, Y.-P.; Wang, J.; Li, Z.; Rohani, S.; Ching, C.-B. *J. Cryst. Growth* **2011**, *335*, 110–114.

(5) Vishweshwar, P.; McMahon, J. A.; Bis, J. A.; Zaworotko, M. J. *J. Pharm. Sci.* **2006**, *95*, 499–516.

(6) MacFhionnghaile, P.; Hu, Y.; Gniado, K.; Curran, S.; McArdle, P.; Erxleben, A. *J. Pharm. Sci.* **2014**, *103*, 1766–1778.

(7) Cuadra, I. A.; Cabanas, A.; Cheda, J. A. R.; Martinez-Casado, F. J.; Pando, C. *J. CO_2 Util.* **2016**, *13*, 29–37.

(8) Munk, T.; Baldursdottir, S.; Hietala, S.; Rades, T.; Kapp, S.; Nuopponen, M.; Kalliomaki, K.; Tenhu, H.; Rantanen, J. *Mol Pharm* **2012**, *9*, 1932–1941.

(9) Serajuddin, A. T. M. *Adv. Drug Deliver. Rev.* **2007**, *59*, 603–616.

(10) Pallipurath, A.; Skelton, J. M.; Delori, A.; Duffy, C.; Erxleben, A.; Jones, W. *CrystEngComm* **2015**, *17*, 7684–7692.

(11) Bucar, D.-K.; Filip, S.; Arhangelskis, M.; Lloyd, G. O.; Jones, W. *CrystEngComm* **2013,** *15*, 6289–6291.

(12) Dongpeng Y.; Delori, A.; Lloyd, G. O.; Friscic, T.; Day, G. M.; Jones, W.; Lu, J.; Wei, M.; Evans, D. G.; Duan, X. *Angew. Chem. Int. Ed.* **2011**, *123*, 12483–12486.

(13) Evora, A. O. L.; Castro, R. A. E.; Maria, T. M. R.; Silva, M. R.; ter Horst, J. H.; Canotilho, J.; Eusebio, M. E. S. *Int. J. Pharm.* **2014**, *466*, 68–75.

(14) Friscic, T.; Childs, S. L.; Rizvi, S. A. A.; Jones, W. *CrystEngComm* **2009**, *11*, 418–426.

(15) Chadwick, K.; Davey, R.; Sadiq, G.; Cross, W.; Pritchard, R. *CrystEngComm* **2009**, *11*, 412–414.

(16) Évora, A. O. L.; Castro, R. A. E.; Maria, T. M. R.; Silva, M. R.; ter Horst, J. H.; Canotilho, J.; Eusébio, M. E. S. *CrystEngComm* **2016**, *18*, 4749–4759.

(17) Evora, A. O. L.; Castro, R. A. E.; Maria, T. M. R.; Rosado, M. T. S.; Silva, M. R.; Matos Beja, A.; Canotilho, J.; Eusebio, M. E. S. *Cryst. Growth Des.* **2011**, *11*, 4780–4788.

(18) Manin, A. N.; Voronin, A. P.; Drozd, K. V.; Manin, N. G.; Bauer-Brandl, A.; Perlovich, G. L. *Eur. J. Pharm. Sci.* **2014**, *65*, 56–64.

(19) Grecu, T.; Adams, H.; Hunter, C. A.; McCabe, J. F.; Portell, A.; Prohens, R. *Cryst. Growth Des.* **2014**, *14*, 1749–1755.

(20) Grecu, T.; Hunter, C. A.; Gardiner, E. J.; McCabe, J. F. *Cryst. Growth Des.* **2014**, *14*, 165–171.

(21) Springuel, G.; Norberg, B.; Robeyns, K.; Wouters, J.; Leyssens, T. *Cryst. Growth. Des.* **2012**, *12*, 475-484.

(22) Hathwar, V. R.; Pal, R.; Row, T. N. G. *Cryst Growth Des.* **2010**, *10*, 3306–3310.

(23) Chan, H. C. S.; Kendrick, J.; Neumann, M. A.; Leusen, F. J. J. *CrystEngComm* **2013**, *15*, 3799–3807.

(24) Fabian, L. Cambridge Structural Database Analysis of Molecular Complementarity in Cocrystals. *Cryst. Growth Des.* **2009**, *9*, 1436–1443.

(25) Macrae, F.; Bruno, I. J.; Chisholm, J. A.; Edgington, P. R.; McCabe, P.; Pidcock, E.; Rodriguez-Monge, L.; Taylor, R.; Streek, J. v. d.; Wood, P. A. Mercury CSD 2.0 - New Features for the Visualization and Investigation of Crystal Structures C. *J. Appl. Cryst* **2008**, 41, 466–470. R.

(26) Delori, A.; Galek, P. T. A.; Pidcock, E.; Jones, W. *Chem. - Eur. J.* **2012**, *18*, 6835–6846.

(27) Delori, A.; Galek, P. T. A.; Pidcock, E.; Patni, M.; Jones, W. *CrystEngComm* **2013**, *15*, 2916–2928.

(28) Etter, M. C. *Acc. Chem. Res.* **1990**, *23*, 120–126.

(29) Lemmerer, A.; Govindraju, S.; Johnston, M.; Motloung, X.; Savig, K. L. *CrystEngComm* **2015**, *17*, 3591–3595.

(30) Kwon, Y. *J. Mol. Struct. -Theochem* **2000**, *532*, 227–237.

(31) Fiedler, P.; Bohm, S.; Kulhanek, J.; Exner, O. *Org. Biomol. Chem.* **2006**, *4*, 2003–2011.

(32) Wang, L.; Tan, B.; Zhang, H.; Deng, Z. *Org. Process Res. Dev.* **2013**, *17*, 1413–1418.

(33) Bag, P. P.; Ghosh, S.; Khan, H.; Devarapalli, R.; Reddy, C. M. *CrystEngComm* **2014**, *16*, 7393–7396.

(34) Surov, A. O.; Voronin, A. P.; Manin, A. N.; Manin, N. G.; Kuzmina, L. G.; Churakov, A. V.; Perlovich, G. L. *Mol. Pharm.* **2014**, *11*, 3707–3715.

(35) Ahn, S.; Matzger, A. J. *J. Am. Chem. Soc.* **2012**, *134*, 3208–3214.

(36) Mukuta, T.; Lee, A. Y.; Kawakami, T.; Myerson, A. S. *Cryst. Growth Des.* **2005**, *5*, 1429–1436.

(37) (a) SHELXT - Sheldrick, G. M. *Acta Crystallogr*. **2015**, *A71*, 3–8. (b) SHELXL - Sheldrick, G. M. *Acta Crystallogr*. **2015**, *C71*, 3–8.

(38) McArdle, P.; Gilligan, K.; Cunningham, D.; Dark, R.; Mahon, M. *CrystEngComm* **2004**, *6*, 303–309.

(39) Hanwell, M. D.; Curtis, D. E.; Lonie, D. C.; Vandermeersch, T.; Zurek, E.; Hutchison, G. R. *J Cheminform.* **2012**, *4*, 17.

(40) Bruno, I. J.; Cole, J. C.; Edgington, P. R.; Kessler, M.; Macrae, C. F.; McCabe, P.; Pearson, J.; Taylor, R. *Acta Cryst.* **2002**, *B58*, 389–397.

(41) Galek, P. T. A.; Chisholm, J. A.; Pidcock, E.; Wood, P. A. *Acta Cryst.* **2014**, *B70*, 91–105.

(42) Gavezzotti, A. *Z. Kristallogr.* **2005**, *220*, 499–510.

(43) Shattock, T. R.; Arora, K. K.; Vishweshwar, P.; Zaworotko, M. J. *Cryst. Growth Des.* **2008**, *8*, 4533–4545.

(44) Goswami, P. K.; Thaimattam, R.; Ramanan, A. *Cryst. Growth Des.* **2016**, *16*, 1268–1281.

(45) Gavezzotti, A.; Colombo, V.; Presti, L. L. *Cryst. Growth Des.* **2016**, DOI: 10.1021/acs.cgd.6b01146.

(46) Cross, W. I.; Blagden, N.; Davey, R. J.; Pritchard, R. G.; Neumann, M. A.; Roberts, R. J.; Rowe, R. C. *Cryst. Growth Des.* **2003**, *3*, 151–158.

(47) Cavallo, G.; Metrangolo, P.; Milani, R.; Pilati, T.; Priimagi, A.; Resnati, G.; Terraneo, G. *Chem. Rev.* **2016,** *116*, 2478–2601.

(48) Arderne, C.; Olivier, D. K.; Ndinteh, D. T. *Acta Cryst.* **2015**, *C71*, 146–151.

(49) Thomas, L. H.; Wales, C.; Zhao, L.; Wilson, C. C. *Cryst. Growth Des.* **2011**, 11, 1450–1452.

(50) Thomas, L. H.; Wales, C.; Wilson, C. C. *Chem. Commun.* **2016**, 52, 7372-7375.

(51) Davey, R. J.; Black, S. N.; Logan, D.; Maginn, S. J.; Fairbrother, J. E.; Grant, D. J. W. *J. Chem. Soc., Faraday Trans.* **1992**, 88, 3461–3466.

(52) Smith, P. E. *Fluid Phase Equilibr.* **2010**, 290, 36–42.

(53) Hu, Y.; Gniado, K.; Erxleben, A.; McArdle, P. *Cryst. Growth Des.* **2014**, *14*, 803–813.

(54) Jones, C. L.; Wilson, C. C.; Thomas, L. H. *CrystEngComm* **2014**, *16*, 5849–5858.

(55) Yuan, X.; Xiang, T.-X.; Anderson, B. D.; Munson, E. J. *Mol. Pharm.* **2015**, *12*, 4512–4528.

Table 1. Crystallographic data for **1a** – **1c**

	1a	**1b**	**1c**
Formula weight	290.24	349.32	382.36
Temperature	299.3(7) K	149.5(8) K	150.1(1) K
Wavelength	0.71073 Å	0.71073 Å	0.71073 Å
Crystal system	triclinic	monoclinic	triclinic
Space group	P-1	$P2_1/c$	P-1
Unit cell dimensions	a = 6.6989(5) Å b = 6.7724(6) Å c = 15.4897(13) Å α = 97.507(7)° β = 97.957(7)° γ = 108.606(7)°	a = 16.4959(13)Å b = 7.4339(5) Å c = 27.064(2) Å α = 90° β = 95.936(7)° γ = 90°	a = 3.8618(2) Å b = 10.9073(7) Å c = 21.1215(14)Å α = 82.528(5)° β = 86.109(5)° γ = 82.588(5)°
Volume	648.05(10) $Å^3$	3301.0(4) $Å^3$	873.56(10) $Å^3$
Z	2	8	2
Density (calculated)	1.487 g/cm^3	1.406 g/cm^3	1.454 g/cm^3
Goodness-of-fit on F^2	1.032	1.098	1.025
R_1 (obs. reflections)	0.0734	0.0469	0.0936
wR_2 (obs. reflections)	0.1547	0.1188	0.1976
Reflections collected	2919	6500	15026
Independent reflections	1926	3974	7615
R (int)	0.0499	0.0188	0.0446

Table 2. Stacking analysis carried out using OSCAIL showing the percentage of atoms in a molecule in vdW contact with potential stack neighbours. A value >50% indicates a significant stacking interaction that will dominate crystal growth.

Crystal	% vdW contact	Crystal habit
1	Along a axis – Mean %** 84.62%	needle (acicular)
1a	Along a axis – Mean %** 42.54% Along c axis – Mean %** 32.69%	diamond-like
1b	Along b axis – Mean %** 21.05%	plate-like
1c	Along a axis- Mean %** 82.01%	needle

Table 3. PIXEL energy calculations (in kJ/mol) for the co-crystal **1a**, showing the contributions from various interactions between **1** and **a**

Symmetry Operation	Fragment	Distance	Coulombic	Polarisability	Dispersion	Repulsion	Pixel
x+1,y,z	diflunisal	6.699	-3.1	-1.6	-17.9	5.6	-17
x-1,y,z	diflunisal	6.699	-3.1	-1.6	-17.9	5.6	-17
x,y+1,z	diflunisal	6.772	-1.1	-1.4	-19.4	7.6	-14.3
x,y-1,z	diflunisal	6.772	-1.1	-1.4	-19.4	7.6	-14.3
x+1,y+1,z	diflunisal	7.86	-1.8	-0.8	-13.2	3.8	-12
x-1,y-1,z	diflunisal	7.86	-1.8	-0.8	-13.2	3.8	-12
x+1,y,z	pyrazine	4.259	-8.7	-3.1	-30.9	22.9	-19.8
x,y,z	pyrazine	7.671	-65.6	-32.3	-18.5	73.3	-43.1

Table 4. Results of crystallisation and balling milling experiments of **1** (FI) with all co-coformers

Co-former	Ball milling	Solution crystallisation
a	co-crystal (identical to the co-crystal obtained from solution)	co-crystal
b	salt (identical to the structure obtained from solution, substoichiometric amounts of solvent required)	salt
c	1:1 and 2:1 co-crystals	salt
d	1:1 and 2:1 co-crystals	**1** (FI)
e	1:1 and 2:1 co-crystals	**1** (FI and FIV) [a]
f	co-crystal	**1** (FI)
g	co-crystal	**1** (FI)
h	X-ray amorphous (stability >6 months)	**1** (FI)
i	Bragg peaks of the acid with an underlying amorphous halo	**1** (FI)
j - s	physical mixtures of **1** and the co-former	**1** (F1)

[a] crystallisation from ethanol

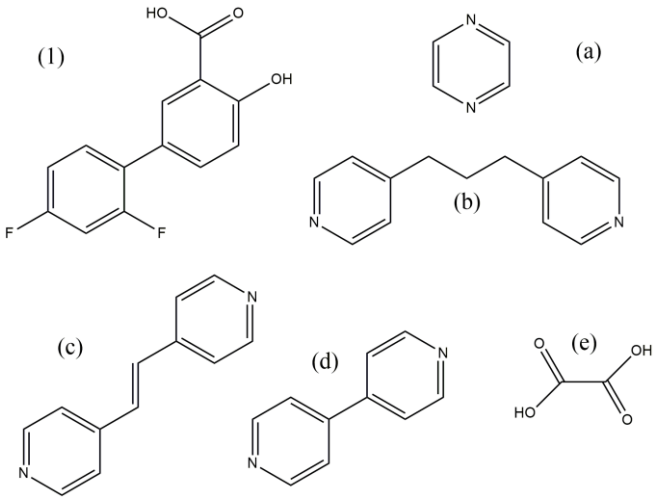

Chart 1. Molecular structures of (1) diflunisal, (a) pyrazine, (b) 1, 3-di (4-pyridyl) propane, (c) 4-(2-pyridine-4-ethyl) pyridine, (d) 4,4'-bipyridine and (e) oxalic acid.

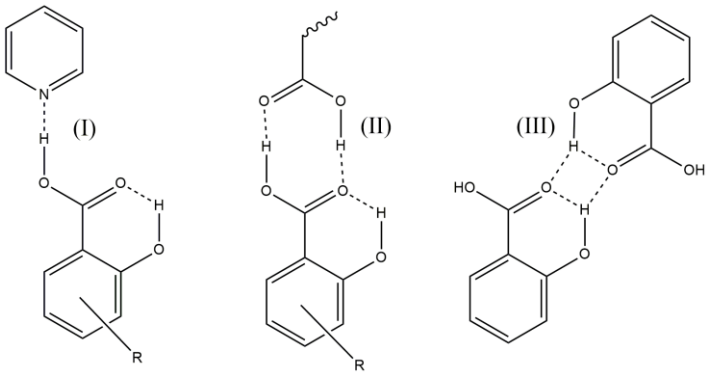

Chart 2. Hydrogen bonding motifs in ortho hydroxy benzoic acids, (I) heterosynthon forming chain like motifs with aromatic N, (II) COOH….COOH homosynthon and (III) homosynthons forming four-atom rings with the ortho OH and the C=O of the acid.

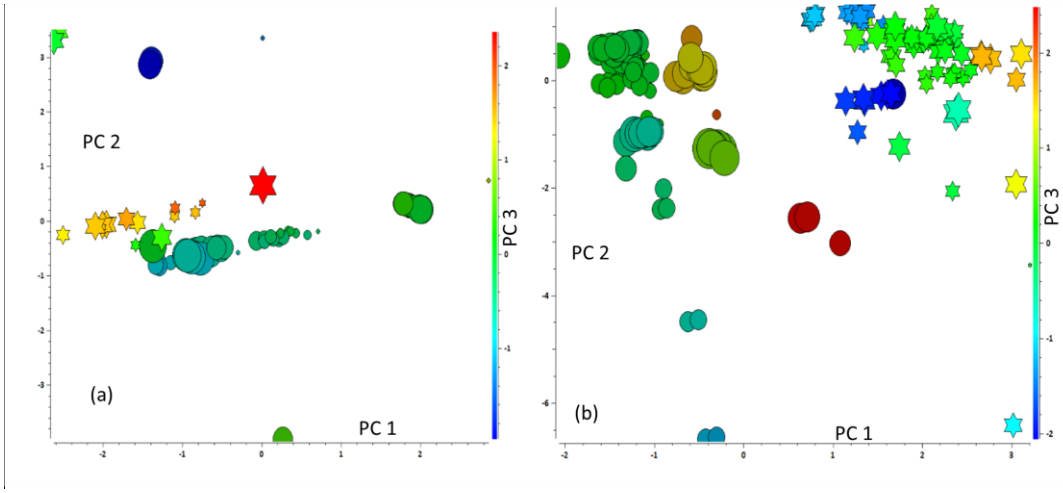

Figure 1. Principal component analysis of the CSD searches for (a) motif I (Chart 2) and (b) motif II (Chart 2). The two axes are PC1 and PC2, with the colour variation given by PC3 and size of the spot by PC4. The 'star' spots are the ones where the interaction distances exclude a planar $R_2^2(8)$ motif.

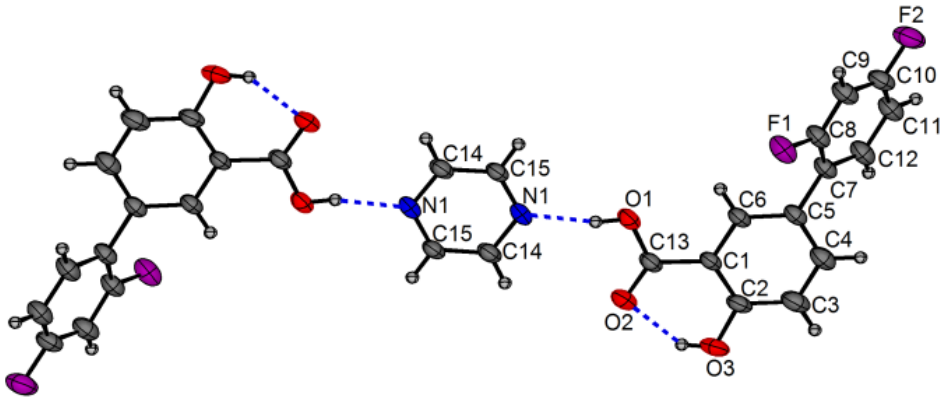

1a

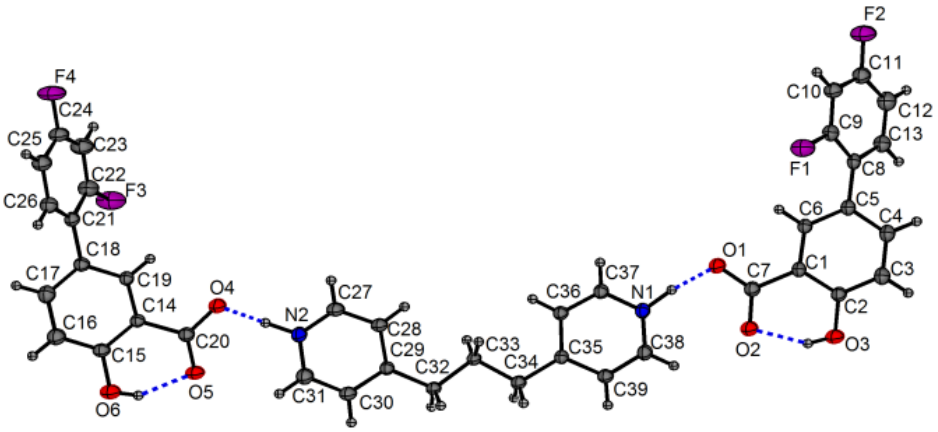

1b

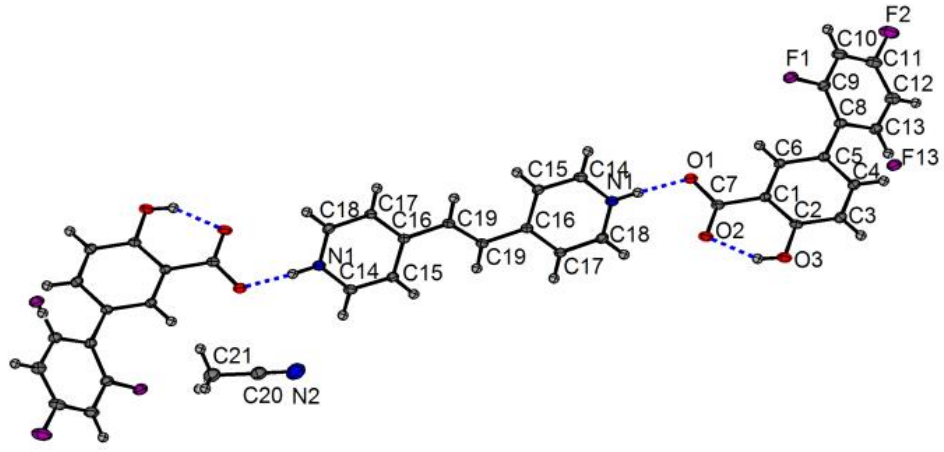

1c

Figure 2. Crystal packing in **1a**, **1b** and **1c**.

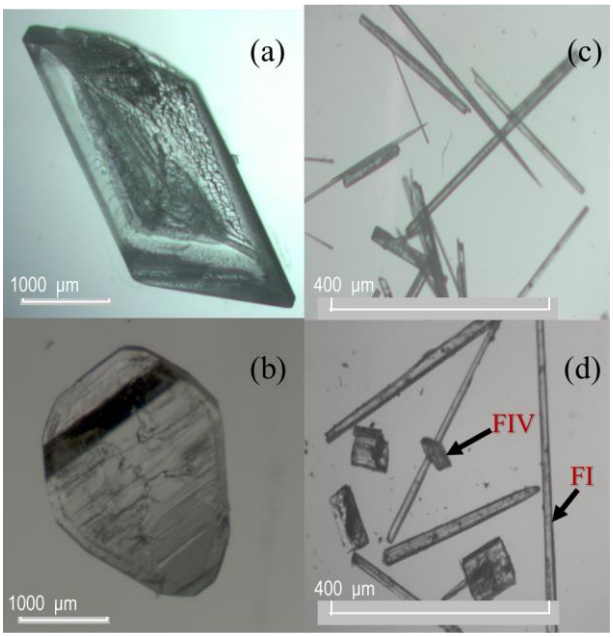

Figure 3. Microscope images of a) **1a**, b) **1b**, c) **1c** and d) Form I and Form IV of **1** crystallised in the presence of oxalic acid.

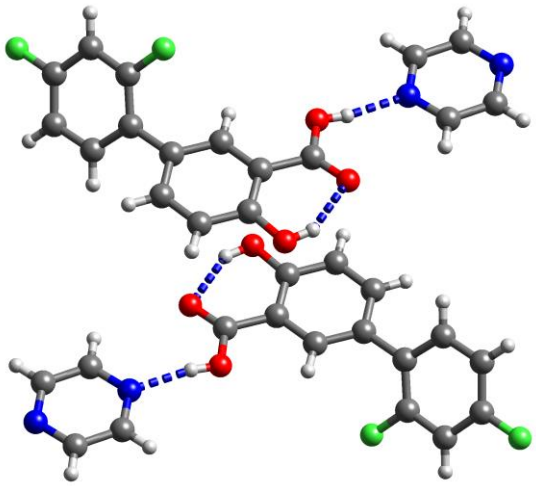

Figure 4. Molecular interactions observed in co-crystal **1a** through PIXEL calculations.

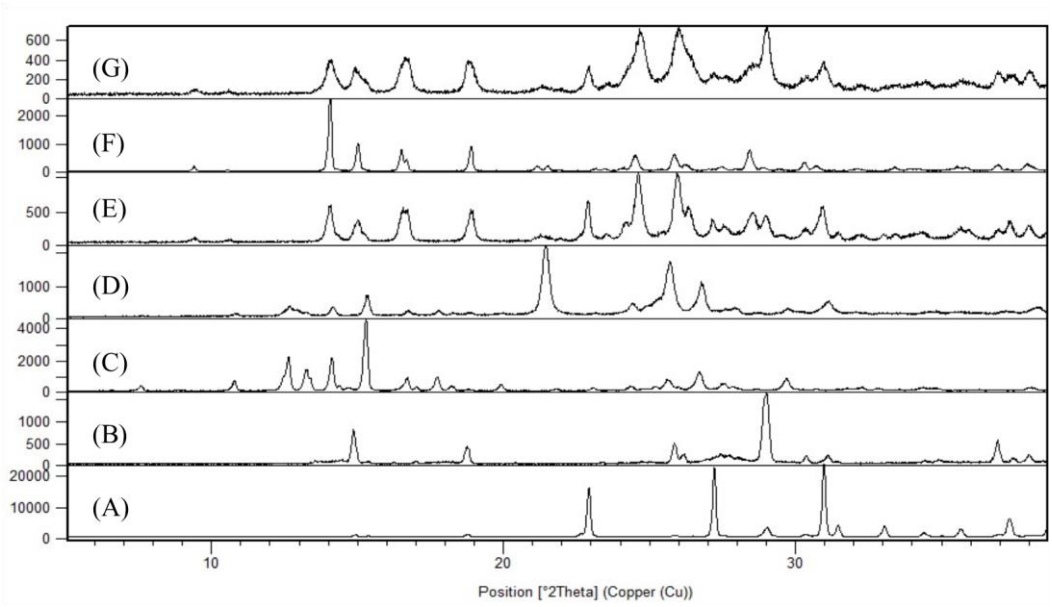

Figure 5. XRPD patterns of milled samples of **1** and OA: (**A**) OA dihydrate. (**B**) OA. (**C**) diflunisal FIII. (**D**) 1:1 mixture of **1** and OA milled continuously for 120 min without cooling. (**E)** co-milled **1** and OA heated at 100 °C for 30 min followed by 30 min at 180 °C. (**F**) co-milled **1** and OA heated at 100 °C for 30 min. (**G**) co-milled **1** and OA (1:1, 60 min). (**D**) shows peaks similar to FIII of **1** and one new peak at 21 ° (2θ). (**G**) shows a new pattern suggesting the presence of a co-crystal.

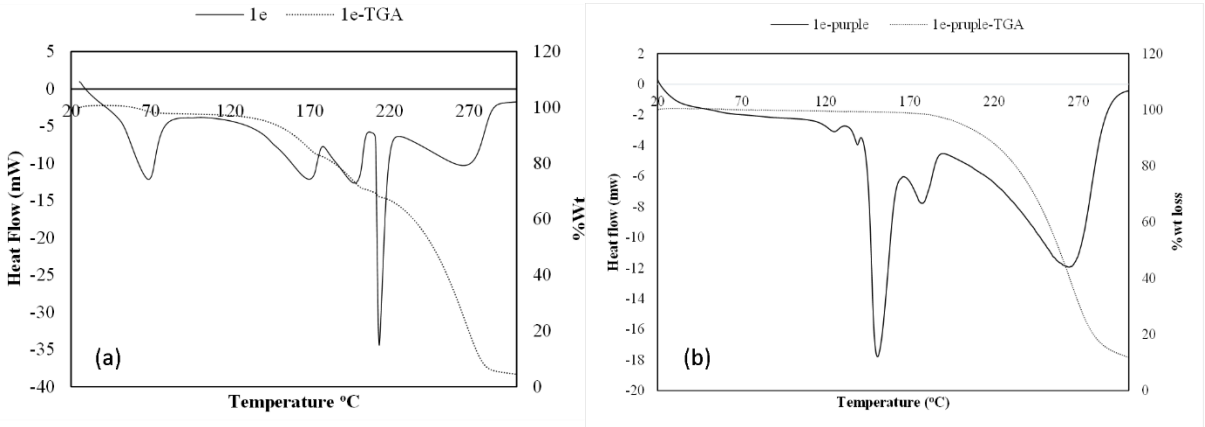

Figure 6. (a) Simultaneous DSC and TGA of a milled sample of **1** and OA (1:1, 30 min) showing thermal events at 67 °C, 171 °C, and 199 °C, with associated weight loss of 1.5%, 15.5% and 27.2%, followed by melting at 213 °C and sublimation of **1** at 262 °C. (b) Simultaneous DSC and TGA of a milled sample of **1** and OA (1:1, 120 min without intermittent cooling) showing thermal events at 126 °C, 143 °C, 151 °C, and 178 °C without weight loss.

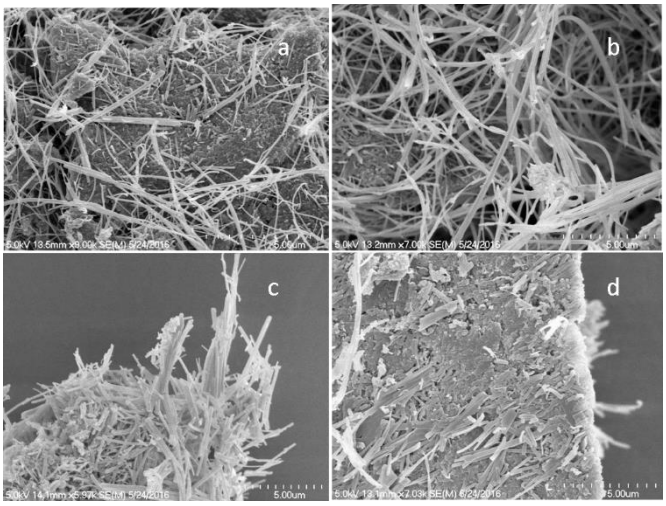

Figure 7. SEM images of (a) co-milled **1** and **d** (2:1, 15 min), (b) co-milled **1** and **f** (1:1, 60 min), (c) co-milled **1** and **f** (2:1, 60 min) and (d) co-milled **1** and **h** (1:1, 30 min).

Figure 8. SEM images of samples of co-milled **1** and **e**: (a) 1:1, 120 min milling, (b) 1:1, 60 min milling followed by heating at 100 °C for 30 min and (c) 1:1, 60 min milling followed by heating at 100 °C for 30 min, followed by heating at 180 °C for 30 min.

Table of Contents use only

Tailoring Co-crystal and Salt Formation and Controlling the Crystal Habit of Diflunisal

Anuradha R. Pallipurath, Francesco Civati, Magdalene Eziashi, Elaf Omar, Patrick McArdle,* and Andrea Erxleben*

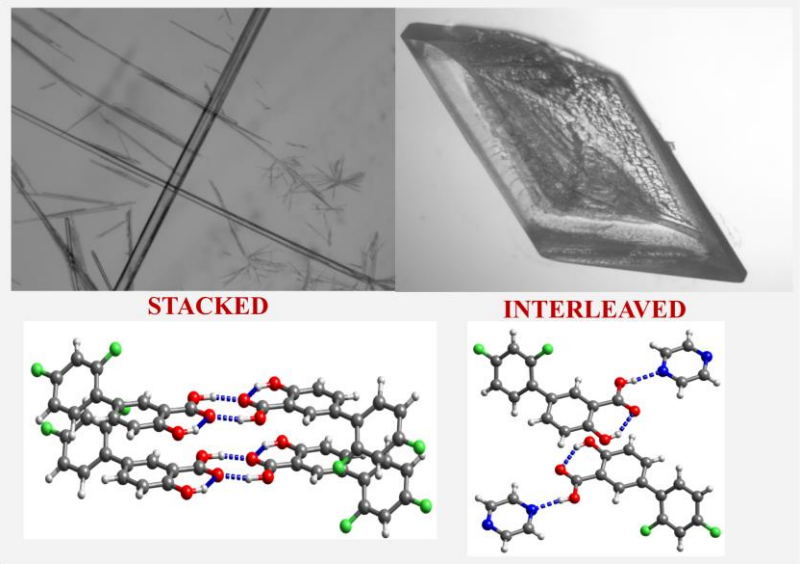

Crystal habit modification through prevention of stacking of molecules and the prevention of disorder in the crystal structures of diflunisal was achieved through co-crystallisation and the formation of CH…F interactions. Eight new co-crystals are reported, along with a statistical analysis of their H-bonding motifs.